JOURNAL OF MATERIALS SCIENCE **40** (2005) 2849–2854

Rapid sintering of ultra-fine WC-10 wt% Co by high-frequency induction heating

H. C. KIM, I. J. SHON
Department of Materials Engineering, The Research Center of Industrial Technology, Engineering Research Institute, Chonbuk National University, Chonbuk 560-756, South Korea

Z. A. MUNIR*
Facility for Advanced Combustion Synthesis, Department of Chemical Engineering and Materials Science, University of California, Davis, California 95616, USA

High-frequency induction-heated sintering (HFIHS) is utilized to consolidate ultra-fine grain WC-10 wt% Co. Densification to near theoretical density in a relatively short time can be accomplished with insignificant change in grain size. WC-10 wt.% Co with a relative density of up to 99.5% was produced within 1 min with the simultaneous application of 60 MPa pressure. The average grain size of the densified material was about 260 nm and the mean free path in the cemented carbide was about 11 nm. The sintered material had fracture toughness and hardness values of 13 $MPa \cdot m^{1/2}$ and 1886 kg/mm^2, respectively. The hardness is comparable to literature values but the fracture toughness is about two times higher. These results are interpreted in terms of current effects on sintering and mass transport. Higher heating rates result in higher density with smaller WC grain size, and higher current-induced solubility of WC in Co is proposed as an explanation for the high fracture toughness.

1. Introduction

The refractory nature of transition element carbides along with their high hardness and thermal and electrical conductivities, make them attractive for applications in the cutting tool industry. Cemented carbides, primarily those of WC have been commonly used in this application and widely investigated. They are formed by sintering of WC powders with the binder (typically Co or Ni) at temperature near the melting point of the metal. The formation of a liquid phase during sintering enhances the densification process and it is the primary motivation for the addition of the binder [1].

Recent increased focus on nanostructured materials has been largely motivated by predicted and demonstrated significant improvements in physical and mechanical properties in such materials [2–5]. Such efforts have included research on cemented carbides. For example, it was demonstrated that nanocrystalline WC-Co cemented carbide powders (with crystallite size of less than 100 nm) could be prepared by a spray conversion process (SCP) [6]. However, when attempts were made to consolidate these powders, the grain size of WC increased significantly due to the fast diffusion through the liquid phase during sintering. The WC grains increased in size from less than 100 nm to 500 nm or larger [6, 7]. Even with the addition of grain growth inhibitors, WC grains size increased up to 300 nm during the process [6–8]. Thus the control of grain growth during sintering remains a technical barrier and is one of the keys to the commercial success of nanostructured WC-Co composites.

The difficulties encountered in the sintering of nanopowders due powder agglomeration have been dealt with by the use of pressure. The application of pressure to accelerate densification is a well-known approach in sintering studies [9, 10] through the use of such methods as hot-pressing, hot-isostatic pressing, hot extrusion, sinter-forging, and spark plasma sintering (SPS) [11]. The applied pressure lowers the vacancy concentration at the grain boundaries (vacancy sinks) relative to the pores (vacancy sources) and thus pore shrinkage and densification rates increase. When high pressure is applied, the contribution of plastic yielding to densification is such that lower temperatures and shorter times are required for the overall compaction process.

In this paper, we report on results of sintering obtained by a new process, high- frequency induction-heating sintering (HFIHS), a method which combines short-time high-temperature exposure with both high-pressure application. The goal of this work is to produce dense nanostructured WC-10 wt% Co cemented carbide.

*Author to whom all correspondence should be addressed.

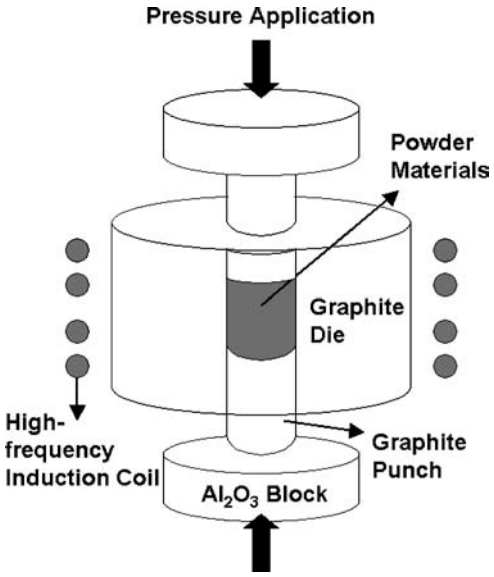

Figure 1 Schematic diagram of apparatus for high-frequency induction-heated sintering.

2. Experimental materials and methods

The tungsten carbide-cobalt powder used in this research was supplied by Nanotech Co. (Cheong-ju, Korea) and was produced by a spray conversion process [6, 12]. The average crystallite size is <200 nm according to the specification by the vendor. The powders were placed in a graphite die (outside diameter, 45 mm; inside diameter, 20 mm; height, 40 mm) and then introduced into the high-frequency induction-heated sintering system, shown schematically in Fig. 1. The system was first evacuated and a uniaxial pressure of 60 MPa was applied. An induced current (frequency of about 50 kHz) was then activated and maintained until densification was observed, as indicating by the observed shrinkage of the sample. Sample shrinkage is measured by a linear gauge measuring the vertical displacement. The induced current was varied from 60 to 90% output of the total power capacity. Under these conditions the sample temperature did not exceed the melting point of cobalt, 1495°C, thus avoiding loss of cobalt through liquid phase extrusion. Temperatures were measured by a pyrometer focused on the surface of the graphite die. At the end of the process, the current was turned off and the sample cooled to room temperature at a rate of about 600°C·min^{-1}. The entire process of densification using the HFIHS technique consists of four major control stages. Typical parameters for the process are presented in Table I. The process was carried out under a vacuum of 4×10^{-2} torr.

The relative density of the sintered samples was measured by the Archimedes method. Microstructural information was obtained from samples after being etched and polished. Etching was accomplished by the use of Murakami's reagent (10 g potassium ferricyanide, 10 g NaOH, and 100 mL water) for 1–2 min at room temperature. Compositional and microstructural analyses of the products were made through X-ray diffraction (XRD), scanning electron microscopy (SEM) with energy dispersive spectroscopy (EDS) and field-emission scanning electron microscopy (FE-SEM). Vickers hardness was measured by performing indentations at a load of 30 kg and a dwell time of 15 s. The structure parameters, i.e. the carbide grain size d_{wc} and the mean free path of the binder phase, λ, were obtained by the linear intercept method [13, 14].

TABLE I Processing parameters of high-frequency induction heated sintering of WC-10 wt% Co hard materials

Parameter	Applied value
Vacuum level	40 mtorr
Applied pressure	60 MPa
Induction heating:	
Frequency	50 kHz
Total power capacity	15 kW
Output of total power	60–90%
Duration	~1 min
Heating rate	950–1500°C·min^{-1}
Cooling rate	600°C·min^{-1}

3. Results and discussion

3.1. Densification behavior and microstructure

The variations of shrinkage displacement and temperature with heating time during sintering of WC-10 wt%Co under 60 MPa pressure and 90% output of total power are shown in Fig. 2. As the induced current is applied, the shrinkage displacement increased slightly with temperature up to about 950°C, and then increased abruptly as the temperature is increased from this value. When the temperature reaches about 1140°C, the densification rate becomes nearly negligible, and as will be seen later, and the samples had densified to 99.4% of theoretical density in about 36 s. Further heating to 1215°C resulted in a small increase in density at this power setting. The temperature pertaining to the onset of densification is consistent with other observations on cemented carbides, reporting temperatures in the range of 800–1000°C [15]. The main densification mechanism for this is carbide particle rearrangement, enhanced by the diffusion and viscous flow of the binder. The nature of the product of sintering is

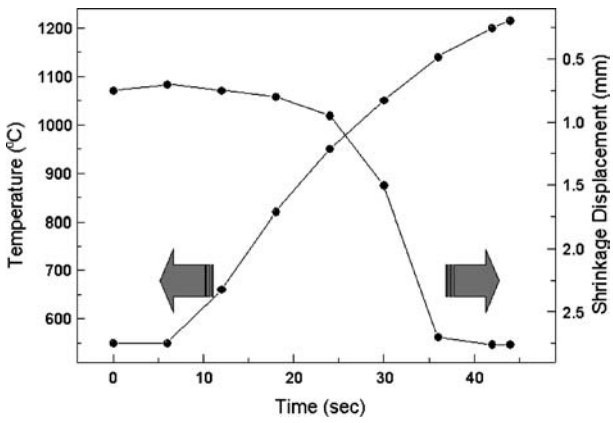

Figure 2 Variations of temperature and shrinkage displacement with heating time during high-frequency induction heated sintering of WC-10 wt% Co hard materials (60 MPa pressure, 90% output of total power capacity).

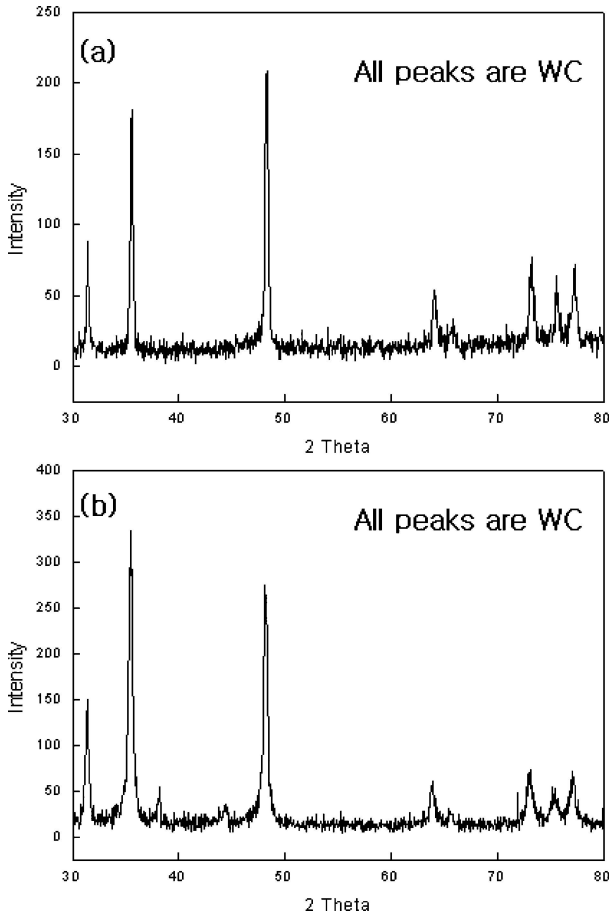

Figure 3 XRD patterns of WC-10 wt% Co hard materials: (a) starting powder and (b) sintered material.

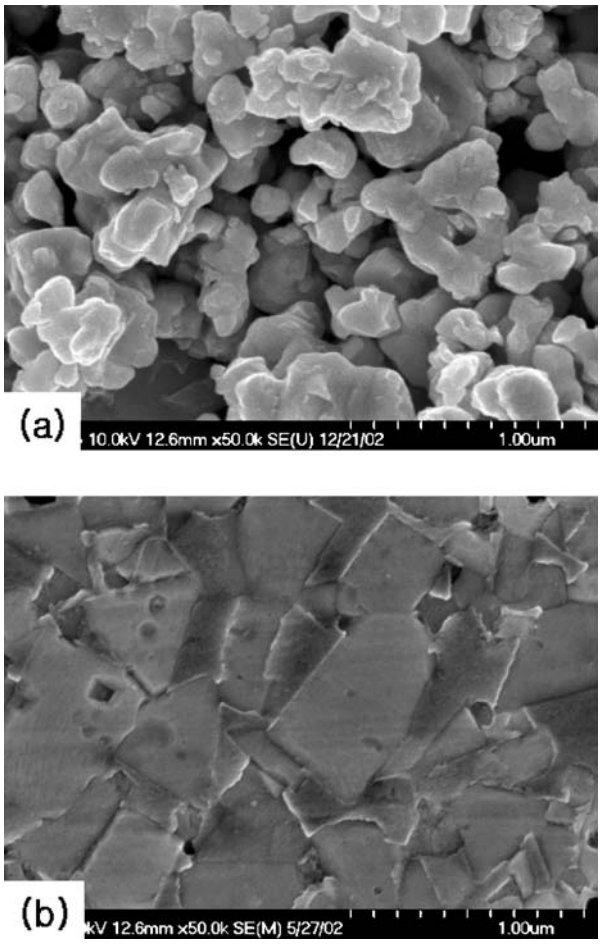

Figure 4 Field Emission Scanning Electron Microscope image of WC-10 wt% Co: (a) starting powder and (b) sintered material.

revealed from Fig. 3, which shows the XRD patterns of WC-10 wt%Co before and after sintering. In both cases only peaks belonging to WC are seen, indicating that no compositional changes took place during sintering. Co peaks are too small to detect, but the presence of this metal is confirmed by X-ray mapping.

FE-SEM images of unsintered and sintered materials are shown in Fig. 4a and b, respectively. The latter, shows an etched surface of a sample heated to 1215°C under a pressure of 60 MPa with a power level of 90%. The WC grains of the unsintered material are round shaped and slightly agglomerated. With sintering at 1215°C (with a total time of induction current application of about 44 s), the cermet exhibits WC grains which are faceted. The average size of these grains in the nearly fully-dense WC-10 wt% Co composite, determined by the linear intercept method, is about 260 nm. Thus the rapid sintering by the HFIHS method had a relatively small effect on grain size, which increased by roughly 30%. The size of WC in the final product obtained in this study is significantly smaller than that obtained by a conventional liquid-phase sintering [8], even though the initial WC grain size of the powders was nearly the same in both cases. The microstructure of WC-10 wt% Co consists of WC crystals embedded in a binder phase. During the sintering process WC crystals develop well-defined crystallographic facets, a process which reflects differences in surface energy of the (010) and (100) planes. Because of this anisotropy, WC grains tends to attain a triangular prism shape, as has been observed before [16].

The attainment of high density in a short time (<1 min) using induction heating with pressure is not well understood. However, similarities between the present method and others, including the spark plasma sintering (SPS) method [17], the electro-discharge compaction method [18], and resistance sintering method [19] are apparent. The role of the current (resistive or inductive) in sintering and or synthesis has been the focus of several attempts aimed at providing an explanation to the observed enhancement of sintering and the improved characteristics of the product. An example of the latter is the observation of clean boundaries in ceramics sintered by the SPS method relative to those obtained by conventional methods [20]. The role played by the current has been variously interpreted, the effect being explained in terms of fast heating rate due to Joule heating, the presence of plasma in pores separating powder particles [21], and the intrinsic contribution of the current to mass transport [22–24]. While evidence for the intrinsic effect is clearly demonstrated, there is no direct evidence for the presence of plasma. Furthermore, the assumed role of pulsing the current in the generation of the plasma and hence the enhancement of densification by its surface cleansing action has not been validated in a recent study [25]. We would therefore suggest that the accelerated HFIHS densification may be attributed to a combination of fast heating

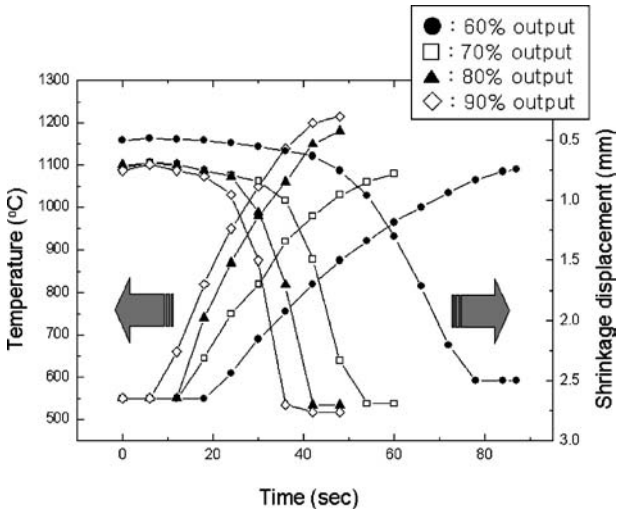

Figure 5 Variation of temperature, shrinkage displacement, and time with output of total power during the sintering of WC-10 wt% Co.

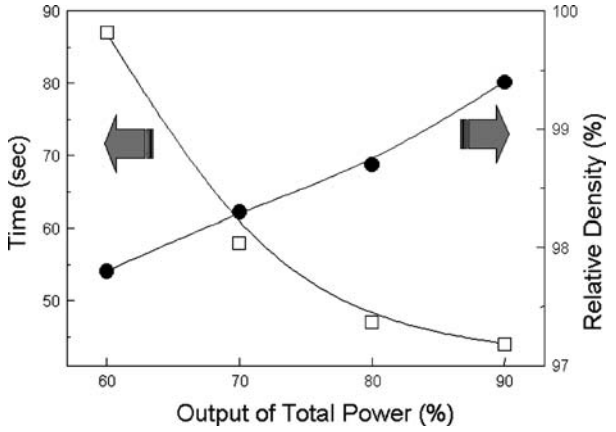

Figure 6 The effect of the power level on the sintering time to achieve maximum density for WC-10 wt% Co.

rates and intrinsic effects on mass transport. Concerning the latter, the solubility of WC in Co is of interest in the present context. The carbide dissolves in cobalt to a relatively significant extent [26]. At 1200°C, for example, the solubility is relatively low, ≤5 mol% [27] while the solubility of Co in WC is extremely small (≤0.5 at%) [28]. It is quite likely that the application of a field enhances the solubility of WC in Co. Solubility enhancement by field application has been demonstrated in a recent study, where it was attributed to a decrease in the free energy of dissolution [29]. This effect will be further discussed in conjunction with the measured properties.

3.2. The effect of power output

The variation of shrinkage displacement and temperature with time for different output of total power capacity during the sintering of WC-10 wt% Co is shown Fig. 5. In all cases, the samples initially experienced a slight shrinkage which was followed by an abrupt increase in shrinkage. The time of the onset of the rapid shrinkage depended on the power level, increasing from about 19 to 42 s as the power level is decreased from 90 to 60%. Correspondingly, the power level had a direct influence on the heating rate, which increased from about 950 to 1500°C · min^{-1} as the power level was increased from 60 to 90%. While the final temperature for a fixed heating time naturally depended on heating rate, the current observations clearly show the effect of heating rate on shrinkage, providing support for one aspect of the role of the current as indicated above.

The effect of the power level on the sintering time to achieve maximum density (from Fig. 5) and on the relative density at that time is shown in Fig. 6. With an increase in the power level, the required time for densification decreases and the relative density increases. Fig. 7 shows SEM (secondary electron) images of the samples sintered at different power level (to the maximum density shown in Fig. 5). The images show a dependence of the WC grain size on the power level (and hence on the heating rate). The grain sizes, as determined by the linear intercept method, were 295, 280, 273, and 260 nm, for materials sintered with power level of 60, 70, 80, and 90%, respectively.

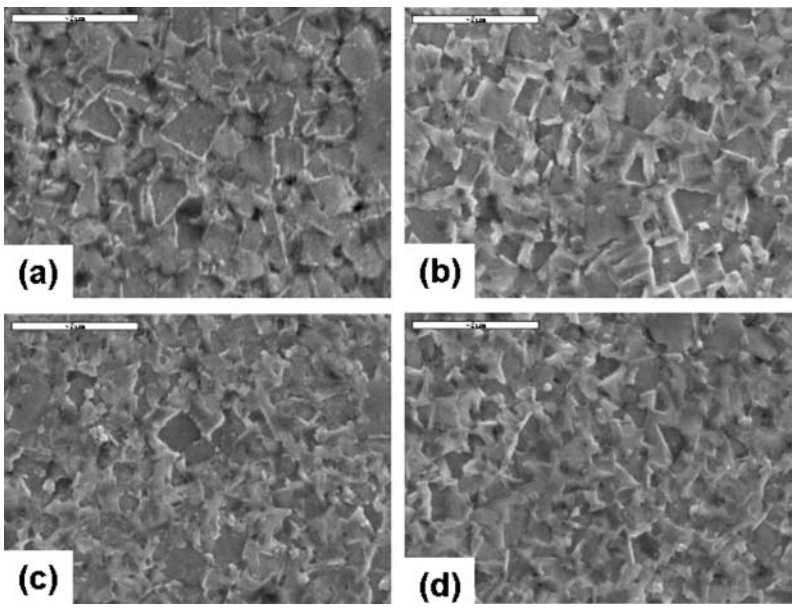

Figure 7 SEM images of WC-10 wt% Co samples sintered to maximum density under power outputs of: (a) 60%, (b) 70%, (c) 80% and (d) 90%.

3.3. Physical and mechanical properties

The Vickers hardness, measured on polished sections using a 30 kg load and 15 s dwell time, was 1886 $kg \cdot mm^{-2}$, a value representing an average of ten measurements. This value is in good agreement with the value 2000 $kg \cdot mm^{-2}$, reported by Richter and Ruthendorf as the maximum value based on literature accounts and on their own work on what they term as "super ultrafine" WC-10 wt% Co (grain size 100–300 nm) [30].

Fracture toughness was calculated from cracks produced in indentations under large loads. The length of these cracks permits an estimation of the fracture toughness of the material by means of Anstis expression [31]. A typical indentation with the radial crack pattern for WC-10 wt% Co composite is shown in Fig. 8a. Higher magnification view of a segment of the indentation radial crack in the composite is shown in Fig. 8b. Typically, one to three additional cracks were observed to propagate radially from the indentation. The calculated fracture toughness value of WC-10 wt% Co composite is about 13 $MPa \cdot m^{1/2}$. As in the case of hardness value, the toughness value is derived from the average of ten measurements. As Fig. 8b shows, crack segments run along the WC-Co phase boundaries. The role of the Co binder phase has been attributed to shielding a stress field in front of crack tip or the bridging of the crack ligaments behind the crack tip [32, 33]. The fracture toughness obtained in this work, 13 $MPa \cdot m^{1/2}$, is more than twice the value reported in the literature for similar materials. Richter and Ruthendorf [30] reported a fracture toughness value of about 6 $MPa \cdot m^{1/2}$ for WC-10 wt% Co with a grain size of 400 nm. Furthermore, for this grain size, there is only a weak correlation between fracture toughness and hardness, in contrast to corresponding observations on WC-Co materials with larger grain sizes, where fracture toughness decreases as harness increases. For small grain size materials (<500 nm), the fracture toughness is nearly independent of Co content [30], implying the lack of an active role by the cobalt layer in hindering the crack propagation. It has been proposed that cobalt behaves in a brittle fashion when the layer thickness (the mean free path) is below a critical value [34].

In view of the observed crack path morphology, the markedly higher fracture toughness value obtained in this work suggests a stronger resistance to crack propagation at the carbide binder interface. The fracture energy along this interface is reported to be lower than that for transgranular fracture [35]. The proposed solubility enhancement of WC in Co, as a result of the application of the field is believed to be responsible for the increased toughness. The tensile strength and ductility of Co is reported to increase with an increase in the content of W and C [36].

The structure parameters, i.e. the carbide grain size d_{wc} and the mean free path of the binder phase λ (the average thickness of the binder phase) are obtained from boundary intercepts with test lines on planar sections. We determined the average number of intercepts per unit length of test line with traces of the carbide/cobalt interface, $N_{WC/Co}$, and of carbide/carbide grain boundaries, $N_{WC/WC}$. From these quantities, we calculated the average carbide grain size and the mean free path using the fallowing relationships [9]:

$$d_{WC} = 2V_{WC}/(2N_{WC/WC} + N_{WC/Co}) \quad (1)$$

$$\lambda = 2V_{Co}/N_{WC/Co} \quad (2)$$

where V_{WC} is the carbide volume fraction and V_{Co} is the binder volume fraction. Fig. 9 shows the Vickers hardness and fracture toughness of WC-10 wt% Co as a function of output of total power. As expected the

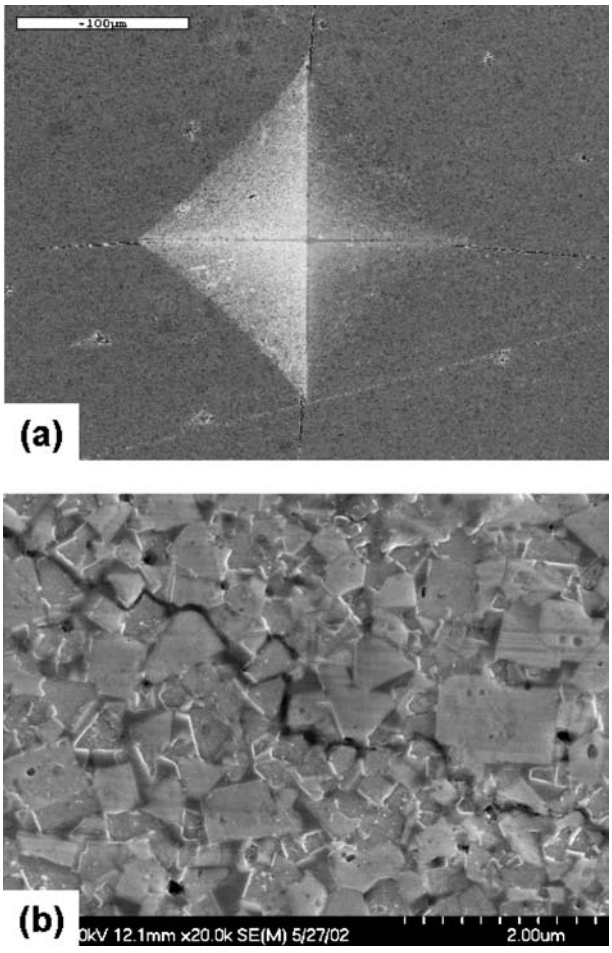

Figure 8 (a) Vickers hardness indentation and (b) radial crack propagating for WC-10 wt% Co.

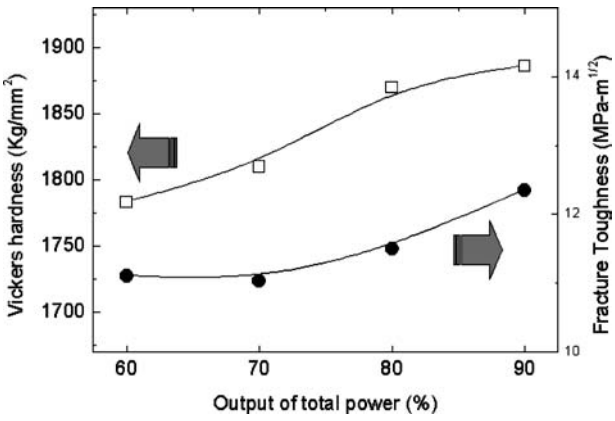

Figure 9 Vickers hardness and fracture toughness as a function of power output (%) for WC-10 wt% Co.

fracture toughness and the hardness increased with increasing output of total power. As the power output increases, the grain size of WC decreases due to the increase in heating rate and the relative density increased. In addition, we would anticipate a higher concentration of WC in Co with higher power. It has been shown that within the temperature range −196 to 900°C, the hardness of WC-Co alloys decreases with increasing WC grain size according to a Hall-Petch type relationship [37].

4. Conclusions

Using high-frequency induction-heated sintering, the densification of WC-10 wt% Co hard materials was accomplished using ultra-fine powders of WC-Co. By this method, complete densification of this material can be achieved within 1 min. The relative density of the composite was 99.5% for an applied pressure of 60 MPa and an induced current of 90% output of total capacity. The WC grain size is about 260 nm and the average thickness of the binder phase is about 11 nm. The fracture toughness and the hardness of WC-10 wt% Co sintered in this study are 13 $MPa{\cdot}m^{1/2}$ and 1886 kg/mm^2, respectively. The hardness is comparable to literature values but the fracture toughness is about two times higher. These results are interpreted in terms of current effects on sintering and mass transport. Higher heating rates result in higher density with smaller WC grain size, and higher current-induced solubility of WC in Co is proposed as an explanation for the high fracture toughness.

Acknowledgements

This work was supported by KISTEP (Korean Institute of Science Technology Evaluation and Planning) through National R&D Project for Nano Science and Technology under the contract # M 10212430001-02B1543-00210 (2002). The support to one of us (ZAM) by the US Army Research Office (ARO) is acknowledged.

References

1. A. HIRATA, H. ZHENG and Y. YOSHIKAWA, *Diamond Related Mater*. **7** (1998) 1669.
2. M. SHERIF EL-ESKANDARANY, *J. Alloys Comp*. **305** (2000) 225.
3. L. FU, L. H. CAO and Y. S. FAN, *Scripta Mater*. **44** (2001) 1061.
4. K. NIIHARA and A. NKAHIRA, "Advanced structural Inorganic Composite" (Elsevier Scientific Publishing Co., Trieste, Italy, 1990).
5. S. BERGER, R. PORAT and R. ROSEN, *Progr. Mater.* **42** (1997) 311.
6. B. K. KIM, G. H. HA and D. W. LEE, *J. Mater. Proc. Tech*. **63** (1997) 317.
7. S. I. CHA, S. H. HONG and B. K. KIM, *Mater. Sci. Eng. A,* (2004) in press.
8. S. I. CHA, S. H. HONG, G. H. HA and B. K. KIM, *Scripta Mater*. **44** (2001) 1535.
9. E. Y. GUTMANAS, in "New Materials by Mechanical Alloying Techniques," edited by E. Arzt and L. Schultz (Oberursel, 1989) p. 129.
10. E. Y. GUTMANAS and A. LAWLEY, "Advan. Powder Metall." edited by E. R. Andreotti and P. J. McGeehan (Princeton, NJ, 1990) Vol. 2 p. 1.
11. M. J. MAYO, D. J. CHEN and D. C. HAGUE, in "Nanomaterials: Synthesis, Properties and Applications," edited by A. S. Edelstein and R. C. Cammarata, (Institute of Physics Pub., 1998) p. 165.
12. B. K. KIM, G. G. LEE, G. H. HA and D. W. LEE, *Met. Mater.* **5** (1999) 109.
13. K. JIA, T. E. FISCHER and G. GALLOIS, *Nanostruct. Mater*. **10** (1998) 875.
14. J. H. HAN and D. Y. KIM, *Acta Mater*. **46** (1998) 2021.
15. A. PETERSON and J. ARGEN, *ibid*. **52** (2004) 1847.
16. S. H. HAN, J. K. PARK, M. Y. HUH and J. KOR, *Powder Metall. Inst.* **6** (1999) 307.
17. U. ANSELMI-TAMBURINI, J. E. GARAY, Z. A. MUNIR, A.TACCA, F. MAGLIA and G. SPINOLO, *J. Mater. Res.* (2004) in press.
18. V. N. BAZANOV, S. A. BALANKIN, J. G. GRIGORIEV, V. V. GUNICHEV, S. V. NOVIKOV and V. A. YARTSEV, in PM'90, PM into the 1990's International Conference on Powder Metallurgy, London 1990 (The Institute of Metals, London 1990) p. 270.
19. C. H. LIU and P. W. KAO, *Scripta Metall. Mater*. **24** (1990) 2279.
20. S. H. RISBUD, J. R. GROZA and M. J. KIM, *Philos. Mag. B* **69** (1994) 525.
21. Z. SHEN, M. JOHNSSON, Z. ZHAO and M. NYGREN *J. Amer. Ceram. Soc.* **85** (2002) 1921.
22. J. E. GARAY, U. ANSELMI-TAMBURINI, Z. A. MUNIR, S. C. GLADE and P. ASOKA-KUMAR, *Appl. Phys. Lett*. **85** (2004) 573.
23. J. R. FRIEDMAN, J. E. GARAY, U. ANSELMI-TAMBURINI and Z. A. MUNIR, *Intermetallics* **12** (2004) 589.
24. J. E. GARAY, U. ANSELMI-TAMBURINI and Z. A. MUNIR, *Acta Materialia* **51** (2003) 4487.
25. W. CHEN, U. ANSELMI-TAMBURINI, J. E. GARAY, J. R. GROZA and Z. A. MUNIR, *Mater. Sci. Eng*. in press (2004).
26. G. GILLE, J. BREDTHAUER, B. GRIES, B. MENDE and W. HEINRICH, *Int J. Refract. Met. Hard Mater*. **18** (2000) 87.
27. O. LAVERGNE, F. ROBAUT, F. HODAJ and C. H. ALLIBERT, *Acta Mater*. **50** (2002) 1683.
28. T. JOHANSSON and B. UHRENIUS, *Met. Sci.* **12** (1978) 83.
29. K. JUNG and H. CONRAD, *J. Mater. Sci*. **39** (2004) 6483.
30. V. RICHTER and M. V. RUTHENDORF, *Int J. Refract. Met. Hard Mater*. **17** (1999) 141.
31. G. R. ANSTIS, P. CHANTIKUL, B. R. LAWN and D. B. MARSHALL, *J. Am. Ceram. Soc*. **64** (1981) 533.
32. L. S. SIGL and H. E. EXNER, *Metall. Trans. A* **18A** (1987) 1299.
33. L. S. SIGL, P. A. MATAGA, B. J. DALGLEISH, R. M. McMEEKING and A. G. EVANS, *Acta Metall*. **36** (1988) 945.
34. G. GILLE, Doctoral thesis, Akademie der Wissenschaften, Germany, 1977.
35. R. SPIEGLER and H. F. FISCHMEISTER, *Acta Met. Mater.* **40** (1992) 1653.
36. B. ROEBUCK, E. A. ALMOND and A. M. COTTENDEN, *Mater. Sci. Eng* **66** (1984) 179.
37. Y. V. MILMAN, S. CHUGUNOVA, V. GONCHARUCK, S. LUYCKX and I. T. NORTHROP, *Int. J. Refract. Met. Hard Mater*. **15** (1997) 97.

Received 4 November 2004
and accepted 5 January 2005